Resolving nonclassical magnon composition of a magnetic ground state via a qubit

Anna-Luisa E. Römling,* Alejandro Vivas-Viaña, Carlos Sánchez Muñoz, and Akashdeep Kamra Condensed Matter Physics Center (IFIMAC) and Departamento de Física Teórica de la Materia Condensada, Universidad Autónoma de Madrid, E-28049 Madrid, Spain

Recently gained insights into equilibrium squeezing and entanglement harbored by magnets point towards exciting opportunities for quantum science and technology, while concrete protocols for exploiting these are needed. Here, we theoretically demonstrate that a direct dispersive coupling between a qubit and a noneigenmode magnon enables detecting the magnonic number states' quantum superposition that forms the ground state of the actual eigenmode - squeezed-magnon - via qubit excitation spectroscopy. Furthermore, this unique coupling is found to enable control over the equilibrium magnon squeezing and a deterministic generation of squeezed even Fock states via the qubit state and its excitation. Our work demonstrates direct dispersive coupling to noneigenmodes, realizable in spin systems, as a general pathway to exploiting the equilibrium squeezing and related quantum properties thereby motivating a search for similar realizations in other platforms.

Introduction.—Quantum superposition is a central concept and ingredient underlying diverse phenomena from entanglement to the quantum speed up in computing [1, 2]. A bosonic mode, such as a photon, can be driven into a so-called nonclassical superposition of its eigenstates - number or Fock states - thereby admitting various quantum advantages [3, 4], such as enhancement in its coupling to a qubit via squeezing [5–9]. At the same time, engineering a dispersive effective interaction $\sim \hat{c}^{\dagger}\hat{c}\hat{\sigma}_z$ between the boson (annihilation operator \hat{c}) and the qubit $\hat{\sigma}_z$ leads to the latter's excitation frequency becoming multivalued and providing information on the boson's wavefunction [10–12]. This has been exploited to measure the quantum superposition of the number states that constitutes a given bosonic state [10, 12–16]. Since such bosons are also the interconnects in quantum computers, this interplay between their nonclassical states and qubits bears a high relevance for emerging quantum technologies [2, 17].

The bosonic spin excitations of magnets, broadly called magnons, potentially offer advantages in realizing quantum properties [15, 18–20]. Magnets have been shown to naturally harbor nonclassical squeezed states in equilibrium [21] arising from an interplay between energy minimization and the Heisenberg uncertainty principle [18, 19, 22]. For example, the ground state and eigenmodes of an anisotropic ferromagnet are constituted by nonclassical superpositions of states with different number of spin flips or, equivalently, magnons [18, 23]. The latter are not the eigenmodes but represent the natural or physical basis for the magnet. Hence, the question arises if and how one can measure such nonclassical superpositions of noneigenmode basis states, that constitute the system eigenmodes. An answer to this is also desirable for harnessing the concomitant equilibrium entanglement harbored by these spin systems for useful quantum information tasks.

In this Letter, taking inspiration from the successful detection of nonequilibrium nonclassical superpositions via a qubit [10, 13–16] and building upon recent advances

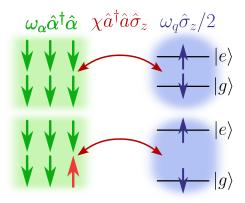


FIG. 1. Schematic depiction of the system. The bosonic uniform magnon mode in a ferromagnet (FM, green) is coupled to a spin qubit (blue) through a spin-spin (e.g., exchange) interaction. The ferromagnetic eigenmode is squeezed-magnon $\hat{\alpha}$, while the qubit $\hat{\sigma}_z$ interacts dispersively with the spin-flip or magnon \hat{a} via $\chi \hat{\sigma}_z \hat{a}^{\dagger} \hat{a}$. This direct dispersive coupling originates from the qubit energy depending on the total FM spin, which is governed by the number of spin-flips or magnons (compare upper and lower panels).

in probing magnets via qubits [13, 15, 16, 24–29], we address the question posed above. We theoretically demonstrate a protocol for measuring the intrinsic nonclassical superposition that forms the squeezed-magnon vacuum ground state of an anisotropic ferromagnet. We find that the conventional qubit spectroscopy employing a coherent qubit-magnon coupling [10, 11, 30] fails in this goal. However, we show that achieving a direct dispersive interaction (Fig. 1) between the qubit and the noneigenmode magnon is the key to achieving this goal. Such a coupling may result from, e.g., the exchange interaction between the magnet and a spin qubit [31, 32]. Furthermore, our proposed qubit-magnon coupling enables a deterministic protocol to generate nonequilibrium squeezed even Fock states [33, 34] by driving the qubit at specific frequencies (Fig. 2).

Direct dispersive coupling between magnon and

qubit.—We consider a ferromagnetic insulator with its equilibrium spin order along the z axis and a spatially uniform (wavevector $\mathbf{k} = \mathbf{0}$) magnonic mode, represented by the annihilation operator \hat{a} . The ferromagnet is coupled to a spin qubit, represented by the operator $\hat{\sigma}_z$, via a spin-spin interaction such as dipolar or exchange coupling (Fig. 1) [35–39]. The $\hat{S}_z\hat{\sigma}_z$ contribution of the spin-spin interaction provides a direct dispersive coupling $\sim \hat{a}^{\dagger}\hat{a}\hat{\sigma}_z$ (see Supplemental Material (SM) [40]). For the moment, we disregard any coherent coupling returning to it later. Due to magnetic anisotropy in the x-y plane, magnons are not the eigenexcitations [22, 36] and the total Hamiltonian reads ($\hbar=1$)

$$\hat{\mathcal{H}}_{\text{sys}} = A\hat{a}^{\dagger}\hat{a} + B\hat{a}^{2} + B^{*}\hat{a}^{\dagger 2} + \frac{\omega_{q}}{2}\hat{\sigma}_{z} + \chi\hat{a}^{\dagger}\hat{a}\hat{\sigma}_{z}$$
 (1)

where A and B parametrize the anisotropic ferromagnet [36] with B resulting from the x-y plane anisotropy, ω_q is the excitation energy of the uncoupled qubit, and χ (assumed positive here) is the direct dispersive coupling strength. A derivation of Eq. (1) is presented in the SM [40].

The ferromagnet only part of the Hamiltonian in Eq. (1) can be diagonalized to $\omega_{\alpha}\hat{\alpha}^{\dagger}\hat{\alpha}$ with $\hat{\alpha}=\hat{a}\cosh r+\hat{a}^{\dagger}\sinh re^{i\theta}$ [22, 36] and

$$\omega_{\alpha} = \sqrt{A^2 - 4 \mid B \mid^2},\tag{2}$$

$$2r = \operatorname{arctanh}\left(\frac{2\mid B\mid}{A}\right). \tag{3}$$

We refer to the eigenmode $\hat{\alpha}$ as bare squeezed-magnon, since it is related to the magnon \hat{a} via the single-mode squeeze operator [3, 22, 36]. The squeezing variables r and θ are determined by A and B of Eq. (1) (see SM [40] for further details), noting that squeezing and r vanish for B=0. As a result, the ferromagnet ground state is vacuum of the squeezed-magnon $\hat{\alpha}$, which is formed by a quantum superposition of the even magnon \hat{a} number states [18, 19]. Since, the \hat{a} magnons are not the eigenmodes, it is not clear how to detect this nonclassical superposition.

Magnon number dependent qubit excitation energy. The nonequilibrium superpositions of eigenmode number states have been investigated via measurement of multiple peaks in a qubit excitation spectroscopy [10, 12, 14]. Here, each peak comes from a different number state contribution to the superposition. Despite a similar motivation, this should be clearly contrasted with our goal and challenge of resolving the noneigenmode magnon number state composition of the equilibrium/eigenmode state the squeezed-magnon vacuum [18, 19, 22]. We hypothesize that the desired resolution can be accomplished in our considered model (Fig. 1) when the qubit energy depends directly on the noneigenmode magnon number $(\sim \chi \hat{a}^{\dagger} \hat{a} \hat{\sigma}_z)$, by spectroscopically probing the qubit excitation energies. We now evaluate the latter to examine this hypothesis.

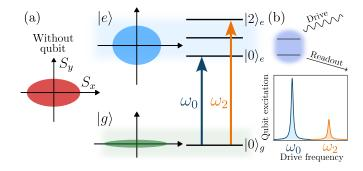


FIG. 2. Qubit excitation spectroscopy of squeezed-magnon (a) The ferromagnet (FM) hosts equilibriumvacuum. squeezed magnons and corresponding vacuums. As a result, the zero-point quantum fluctuations depicted in the spin phase space bear elliptical profiles [18], indicative of their squeezing. The degree of squeezing is different in three cases: (i) qubit not coupled to the FM (red), (ii) qubit in excited state $|e\rangle$ (blue), and (iii) qubit in ground state $|g\rangle$ (green). When one spectroscopically probes the qubit excitation energy $(|q\rangle \rightarrow |e\rangle)$, the squeezed-magnon number can change from 0 to any number state available in the superposition, due to the differing magnon-squeezings in the qubit excited and ground states. (b) This effectively allows to probe the squeezed-magnon vacuum as a superposition of even magnon number states, with each peak (only first two depicted here) in the qubit excitation spectroscopy measuring a term in the superposition.

We first project the total Hamiltonian Eq. (1) onto the qubit ground state $|g\rangle$. The reduced Hamiltonian $\hat{\mathcal{H}}_q = \langle g|\,\hat{\mathcal{H}}_{\mathrm{sys}}\,|g\rangle$ is obtained as

$$\hat{\mathcal{H}}_g = (A - \chi) \,\hat{a}^{\dagger} \hat{a} + B \hat{a}^2 + B^* \hat{a}^{\dagger 2} - \frac{\omega_q}{2} \,. \tag{4}$$

In a direct analogy with the discussion and analysis following Eq. (1), the reduced Hamiltonian Eq. (4) can be diagonalized to $\omega_{\alpha}^{g} \hat{\alpha}_{q}^{\dagger} \hat{\alpha}_{g}$ with a different squeezedmagnon $\hat{\alpha}_q$ eigenmode characterized by a frequency $\omega_{\alpha}^g <$ ω_{α} and squeezing factor $r_q > r$. ω_{α}^g and r_q are obtained from Eqs. (2) and (3) by substituting $A \to A - \chi$ [41]. We will refer to $\hat{\alpha}_q$ as the ground state squeezed-magnon harboring a different magnetic vacuum as compared to the isolated ferromagnet [Fig. 2(a)]. The projection $\mathcal{H}_e = \langle e | \mathcal{H}_{\text{sys}} | e \rangle$ onto the qubit excited state $| e \rangle$ can be obtained from Eq. (4) by changing the sign of χ and ω_q . Analogous to the discussion above, the bosonic eigenmode of $\hat{\mathcal{H}}_e$ becomes the excited state squeezed-magnon $\hat{\alpha}_e$ characterized by eigenenergy $\omega_{\alpha}^e>\omega_{\alpha}$ and squeezing factor $r_e < r$ [Fig. 2(a)], with ω_{α}^e and r_e obtained from Eqs. (2) and (3) on replacing $A \to A + \chi$.

Altogether, we have diagonalized our Hamiltonian Eq. (1) denoting the eigenstates by $|n\rangle_e$ and $|n\rangle_g$, where the subscript g or e indicates the qubit state and $n\in\mathbb{N}$ labels the different Fock states. The key point is that the magnonic eigenmodes and their respective squeezing are different in three cases: (i) isolated ferromagnet, (ii)

qubit in its ground state, and (iii) qubit in its excited state [see Fig. 2(a)].

The typical qubit excitation spectroscopy measures qubit energy corresponding to the transition $|q\rangle \rightarrow |e\rangle$, while the boson number state remains the same [10, 11]. Consequently, when we have a nonequilibrium superposition of multiple number states, the result is observation of boson number-dependent qubit energy that manifests itself as multiple spectroscopy peaks. In sharp contrast, our system has a boson mode whose squeezing depends on the qubit state. Hence, the excitation of qubit need not preserve the boson number. Thus, transitions $|0\rangle_g\,\rightarrow\,|n\rangle_e$ will take place with probability $p_n = |c_n|^2 \equiv \left| e \langle n|0 \rangle_g \right|^2$ resulting in correspondingly high spectroscopy peaks. As demonstrated in the SM [40], the ground state $|0\rangle_q$ is squeezed with respect to the excited state squeezed-magnon vacuum $|0\rangle_e$ with effective squeezing factor of $r_{\text{eff}} = r_g - r_e$ [Eq. (3)]. Thus, we may express $|0\rangle_q = \sum_n c_n |n\rangle_e$ with [3, 4]

$$c_{2n} = \frac{1}{\sqrt{\cosh r_{\text{eff}}}} \left(-e^{i\theta} \tanh r_{\text{eff}} \right)^n \frac{\sqrt{(2n)!}}{2^n n!}$$
 (5)

and $c_{2n+1} = 0$ for $n \in \mathbb{N}$. To sum up, the qubit spectroscopy should yield a peak for each of the superposition contributions [Fig. 2(b)], as intuitively hypothesized above. However, it resolves the ground state squeezed-magnon vacuum $|0\rangle_g$ in terms of the excited state squeezed-magnon number states $|n\rangle_e$ [Eq. (5)].

In Fig. 3(a), we plot the squeezing factors r_g , r_e and $r_{\rm eff}$ as a function of the dispersive coupling strength χ . Only at a certain value of χ , $r_{\rm eff}$ is equal to the squeezing r of the bare squeezed-magnon. In this case, the spectroscopy would probe the "true" distribution of the bare squeezed-magnon $\hat{\alpha}$ vacuum in terms of the magnon $\hat{\alpha}$ Fock states. Nevertheless, employing our analysis above, a knowledge of χ and ω_{α} allows one to translate an observed superposition into any desired basis.

We now examine the position of the spectroscopy peaks. As per energy conservation, the transition $|0\rangle_g \rightarrow |2n\rangle_e$ occurs when the drive frequency matches the energy difference between the two states. As detailed in the SM [40], this is evaluated as ω_{2n} :

$$\omega_{2n} = \omega_q + \frac{\omega_\alpha^e - \omega_\alpha^g}{2} - \chi + 2n \cdot \omega_\alpha^e. \tag{6}$$

For $\chi \ll \min[|A|, ||B| (A/2 |B| - 2 |B| /A)|]$, Eq. (6) becomes $\omega_{2n} \approx \omega_q + 2\chi \cdot \sinh^2 r + 2n [\omega_\alpha + \chi \cosh (2r)]$. The different peaks are now well separated by multiples of the bare squeezed-magnon frequency ω_α , potentially making them easier to detect [42].

In order to guide and quantify the measurability of multiple peaks resulting from the superpositions, we define "contrast" as the ratio $c = p_2/p_0$ evaluating it as

$$2c = \tanh^2(r_{\text{eff}}). \tag{7}$$

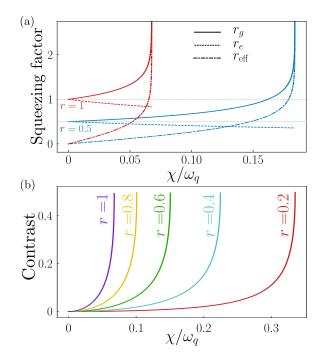


FIG. 3. (a) Squeezing factors vs. χ for the magnonic eigenmodes in the qubit ground state r_g (solid), the qubit excited r_e (dotted) and effective squeezing $r_{\rm eff}=r_g-r_e$ (dashed) considering bare magnon squeezing of r=0.5 (blue) and r=1 (red). (b) Contrast $c=p_2/p_0$ [Eq. (7)] as a function of χ for several values of the squeezing factor r. Its vanishing in the limit $r\to 0$ signifies that more than 1 peak in the spectroscopy is observed only for nonzero magnon squeezing. We consider $\omega_\alpha/\omega_q=0.5$ here.

The contrast c, plotted in Fig. 3(b), generally characterizes the reduction of subsequent peaks expected in the qubit spectroscopy. For small coupling strengths $|\chi| \ll \min{[|A|,|A(A/2|B|-2|B|/A)|]}$, we obtain $c \approx 2|B|^2\chi^2/\left(A^2-4|B|^2\right)^2$. For small $|B| \ll \min{[|A-\chi|,|A+\chi|]}$ and thus squeezing, the contrast can be expanded as $c \approx 2\chi^2|B|^2/\left(A^2-\chi^2\right)^2$. Thus, the equilibrium superposition peaks can be observed in the qubit spectroscopy when both the direct dispersive interaction strength χ and squeezing r are nonzero, with the resolvability of the peaks increasing with both these parameters.

Simulation of qubit spectroscopy.—We now corroborate and complement our analytic considerations above by simulating a qubit spectroscopy setup using the QuTip package [43, 44]. While different experimental methods can be employed to probe the qubit excitation energy [10, 14], here we consider a microwave qubit drive described by $\hat{\mathcal{H}}_{\rm d} = \Omega_d \cos{(\omega_d t)} (\hat{\sigma}_+ + \hat{\sigma}_-)$ where Ω_d denotes the Rabi frequency quantifying the drive strength, while ω_d becomes the drive frequency. As detailed in the SM [40], we consider Eq. (1) and $\hat{\mathcal{H}}_{\rm d}$ to describe our system and account for qubit dissipation [45] via one collapse

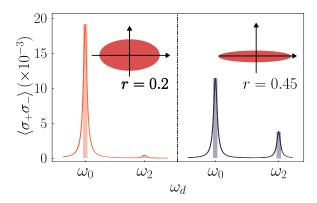


FIG. 4. Numerical simulation of qubit spectroscopy using a Rabi drive. Steady state qubit excitation $\langle \hat{\sigma}_{+} \hat{\sigma}_{-} \rangle$ is plotted against the Rabi drive frequency ω_{d} for two different values of bare magnon-squeezing r. The first two qubit excitation frequencies ω_{0} and ω_{2} are observed. The shaded bars depict the analytically evaluated excitation distributions [Eqs. (5) and (6)], underlining their good agreement with the simulations. Parameters employed in the simulation are $\omega_{\alpha}/\omega_{q}=0.5$, $\chi/\omega_{q}=0.2$, $\gamma_{q}/\omega_{q}=0.1$ and $\Omega_{d}/\omega_{q}=0.014$. The numerical method is detailed in the SM [40].

operator $\hat{C} = \sqrt{\gamma_q} \hat{\sigma}_-$ with qubit decay rate γ_q . Solving the Lindblad master equation [45–47] numerically, we investigate the steady state qubit excitation $\langle \hat{\sigma}_+ \hat{\sigma}_- \rangle$. Ω_d is chosen small enough (see SM [40] for a quantification of this smallness) for the qubit excitation to remain small and in the linear regime [40, 45]. With this protocol, the qubit excitation should manifest a peak whenever the drive frequency ω_d is resonant with a qubit excitation transition.

In Fig. 4, we show simulations (solid curves) of the qubit spectroscopy for two squeezing factors r=0.2 and r=0.45, comparing them with our analytic results plotted as bars at $\omega_d=\omega_{2n}$ [Eq. (6)] with heights $\propto p_{2n}=|c_{2n}|^2$ [Eq. (5)]. Thus, our analytics agree well with the simulations. We therefore conclude that the first non-trivial peak indeed stems from the equilibrium squeezing. Due to a large separation ($\sim \omega_{\alpha}$) between the peaks, experiments may further employ higher values of the drive Ω_d in measuring the smaller peaks. We demonstrate this point explicitly by simulating the ω_4 peak in SM [40].

Consideration of coherent coupling.—Until now, we have considered a magnet coupled to a spin qubit that offers a direct dispersive coupling χ [Eq. (1)], found to be essential for the key phenomena addressed here. We now examine the role of coherent or Rabi interaction [48] parameterized by g, such that the system Hamiltonian becomes:

$$\hat{\mathcal{H}}_{\text{sys,SC}} = A\hat{a}^{\dagger}\hat{a} + B\hat{a}^{2} + B^{*}\hat{a}^{\dagger 2} + \frac{\omega_{q}}{2}\hat{\sigma}_{z} + g\left(\hat{a}^{\dagger} + \hat{a}\right)\left(\hat{\sigma}_{+} + \hat{\sigma}_{-}\right). \tag{8}$$

This interaction is universally present in qubits, such as

with spin [31, 32] and superconducting qubits [29, 30, 49], while the direct dispersive coupling is not always available. When the boson and qubit are strongly detuned i.e., $g \ll |\omega_q - \omega_\alpha|$, the coherent coupling also results in an effective dispersive interaction $\sim \tilde{\chi} \hat{\alpha}^\dagger \hat{\alpha} \hat{\sigma}_z$ [3, 10, 11, 40, 50] which has been exploited in observing nonequilibrium superpositions in terms of the eigenmode number states. It is not clear whether one can employ this effective dispersive coupling to resolve an equilibrium superposition.

Via numerical simulations of qubit spectroscopy employing Eq. (8) (see SM [40]), we find that the effective dispersive interaction $\sim \tilde{\chi} \hat{\alpha}^{\dagger} \hat{\alpha} \hat{\sigma}_z$ does not resolve the nonclassical magnon composition of the equilibrium squeezed-magnon vacuum. This can be understood a posteriori since such an effective coupling may address only the eigenmodes $\hat{\alpha}$, and not any internal noneigenmodes. Thus, a direct dispersive interaction $\sim \chi \hat{a}^{\dagger} \hat{a} \hat{\sigma}_z$ offered by, e.g., a spin qubit is needed for resolving equilibrium superpositions. We also show that any influence of the coherent coupling g when employing a spin qubit system can be suppressed via an adequately large detuning $|\omega_q - \omega_\alpha|$ [40, 50].

Discussion.—In the conventional qubit spectroscopy for dispersively sensing a nonequilibrium quantum superposition of eigenmode Fock states, the peaks are separated in frequency by $\sim \tilde{\chi}$ which is typically small [10–12]. In our demonstrated protocol for detecting the equilibrium superposition of noneigenmode Fock states, the corresponding peaks are well-separated $\sim \omega_{\alpha}$, which makes it feasible to detect them [51] even when they are relatively small (see SM [40]).

The direct dispersive interaction results from the $\hat{S}_z\hat{\sigma}_z$ term contained in exchange as well as dipolar spin-spin interaction hosted by multiple magnet–spin qubit platforms, as discussed in SM [40]. The resulting χ offered by an exchange-coupled spin qubit can be large \sim GHz for small size of the magnet (see the SM [40]) making our proposal better suited for nanomagnets. Furthermore, detection of the nth nontrivial peak in the qubit spectroscopy is accompanied by the transition $|0\rangle_g \rightarrow |2n\rangle_e$ which provides a new deterministic approach to generate nonequilibrium squeezed Fock states $(|2n\rangle_e = S^{-1}(r_{\rm eff})\,|2n\rangle_g$ [18, 22, 33, 34]) by driving the qubit.

Conclusion.—We have theoretically demonstrated how a direct dispersive interaction between a qubit and a noneigenmode boson (here, a magnon) enables detection of the quantum superposition that makes up the actual eigenmodes (here, squeezed-magnon and its vacuum). The same coupling is shown to allow for a control of the equilibrium magnon squeezing and a deterministic generation of squeezed even Fock states via the qubit state and its resonant excitation. Thus, this direct dispersive interaction, readily available in spin systems, opens new avenues for exploiting the equilibrium squeezing and entanglement harbored by magnets. At the same

time, our work inspires a search for the realization of direct dispersive interaction in other, such as optical [52] and mechanical, platforms that could enable access to equilibrium superpositions.

Acknowledgements.—We thank Frank Schlawin for valuable discussions. We acknowledge financial support from the Spanish Ministry for Science and Innovation - AEI Grant CEX2018-000805-M (through the "Maria de Maeztu" Programme for Units of Excellence in R&D) and grant RYC2021-031063-I funded by MCIN/AEI/10.13039/501100011033 and "European Union Next Generation EU/PRTR". A. E. R. acknowledges that the project that gave rise to these results received the support of a fellowship from "la Caixa" Foundation (ID 100010434). The fellowship code is LCF/BQ/DI22/11940029. C. S. M. acknowledges that the project that gave rise to these results received the support of a fellowship from "la Caixa" Foundation (ID 100010434) and from the European Union's Horizon 2020 research and innovation programme under the Marie Skłodowska-Curie Grant Agreement No. 847648, with fellowship code LCF/BQ/PI20/11760026, and financial support from the Proyecto Sinérgico CAM 2020 Y2020/TCS-6545 (NanoQuCo-CM).

- * anna-luisa.romling@uam.es
- S. Wehner, D. Elkouss, and R. Hanson, Quantum internet: A vision for the road ahead, Science 362, eaam9288 (2018).
- [2] A. Laucht, F. Hohls, N. Ubbelohde, M. F. Gonzalez-Zalba, D. J. Reilly, S. Stobbe, T. Schröder, P. Scarlino, J. V. Koski, A. Dzurak, C.-H. Yang, J. Yoneda, F. Kuemmeth, H. Bluhm, J. Pla, C. Hill, J. Salfi, A. Oiwa, J. T. Muhonen, E. Verhagen, M. D. LaHaye, H. H. Kim, A. W. Tsen, D. Culcer, A. Geresdi, J. A. Mol, V. Mohan, P. K. Jain, and J. Baugh, Roadmap on quantum nanotechnologies, Nanotechnology 32, 162003 (2021).
- [3] C. Gerry, P. Knight, and P. L. Knight, *Introductory Quantum Optics* (Cambridge University Press, 2005).
- [4] D. Walls and G. J. Milburn, eds., Quantum Optics (Springer, Berlin, Heidelberg, 2008).
- [5] D. F. Walls, Squeezed states of light, Nature 306, 141 (1983).
- [6] C. Leroux, L. C. G. Govia, and A. A. Clerk, Enhancing Cavity Quantum Electrodynamics via Antisqueezing: Synthetic Ultrastrong Coupling, Physical Review Letters 120, 093602 (2018).
- [7] W. Qin, A. Miranowicz, P.-B. Li, X.-Y. Lü, J. Q. You, and F. Nori, Exponentially Enhanced Light-Matter Interaction, Cooperativities, and Steady-State Entanglement Using Parametric Amplification, Physical Review Letters 120, 093601 (2018).
- [8] S. C. Burd, R. Srinivas, H. M. Knaack, W. Ge, A. C. Wilson, D. J. Wineland, D. Leibfried, J. J. Bollinger, D. T. C. Allcock, and D. H. Slichter, Quantum amplification of boson-mediated interactions, Nature Physics 17, 898 (2021).

- [9] S. Zeytinoğlu, A. İmamoğlu, and S. Huber, Engineering Matter Interactions Using Squeezed Vacuum, Physical Review X 7, 021041 (2017).
- [10] D. I. Schuster, A. A. Houck, J. A. Schreier, A. Wallraff, J. M. Gambetta, A. Blais, L. Frunzio, J. Majer, B. Johnson, M. H. Devoret, S. M. Girvin, and R. J. Schoelkopf, Resolving photon number states in a superconducting circuit, Nature 445, 515 (2007).
- [11] M. Boissonneault, J. M. Gambetta, and A. Blais, Dispersive regime of circuit QED: Photon-dependent qubit dephasing and relaxation rates, Physical Review A 79, 013819 (2009).
- [12] R. Bianchetti, S. Filipp, M. Baur, J. M. Fink, M. Göppl, P. J. Leek, L. Steffen, A. Blais, and A. Wallraff, Dynamics of dispersive single-qubit readout in circuit quantum electrodynamics, Physical Review A 80, 043840 (2009).
- [13] D. Lachance-Quirion, Y. Tabuchi, S. Ishino, A. Noguchi, T. Ishikawa, R. Yamazaki, and Y. Nakamura, Resolving quanta of collective spin excitations in a millimeter-sized ferromagnet, Science Advances 3, e1603150 (2017).
- [14] S. Kono, Y. Masuyama, T. Ishikawa, Y. Tabuchi, R. Ya-mazaki, K. Usami, K. Koshino, and Y. Nakamura, Non-classical photon number distribution in a superconducting cavity under a squeezed drive, Phys. Rev. Lett. 119, 023602 (2017).
- [15] D. Lachance-Quirion, Y. Tabuchi, A. Gloppe, K. Usami, and Y. Nakamura, Hybrid quantum systems based on magnonics, Applied Physics Express 12, 070101 (2019).
- [16] D. Xu, X.-K. Gu, H.-K. Li, Y.-C. Weng, Y.-P. Wang, J. Li, H. Wang, S.-Y. Zhu, and J. Q. You, Quantum control of a single magnon in a macroscopic spin system, Phys. Rev. Lett. 130, 193603 (2023).
- [17] B. M. Terhal, J. Conrad, and C. Vuillot, Towards scalable bosonic quantum error correction, Quantum Science and Technology 5, 043001 (2020).
- [18] A. Kamra, W. Belzig, and A. Brataas, Magnon-squeezing as a niche of quantum magnonics, Applied Physics Letters 117, 090501 (2020).
- [19] H. Y. Yuan, Y. Cao, A. Kamra, R. A. Duine, and P. Yan, Quantum magnonics: When magnon spintronics meets quantum information science, Physics Reports Quantum Magnonics: When Magnon Spintronics Meets Quantum Information Science, 965, 1 (2022).
- [20] D. D. Awschalom, C. R. Du, R. He, F. J. Heremans, A. Hoffmann, J. Hou, H. Kurebayashi, Y. Li, L. Liu, V. Novosad, J. Sklenar, S. E. Sullivan, D. Sun, H. Tang, V. Tyberkevych, C. Trevillian, A. W. Tsen, L. R. Weiss, W. Zhang, X. Zhang, L. Zhao, and Ch. W. Zollitsch, Quantum Engineering With Hybrid Magnonic Systems and Materials (Invited Paper), IEEE Transactions on Quantum Engineering 2, 1 (2021).
- [21] We emphasize the focus of this work on equilibrium squeezed-magnons and their ground state vacuum (e.g., see [18, 19, 22, 53–58]). These are qualitatively distinct from the squeezed states of magnons generated in nonequilibrium via some drives. There also exists much interest in and excitement about such nonequilibrium quantum states of magnons (e.g., see [19, 59–63]).
- [22] A. Kamra and W. Belzig, Super-Poissonian Shot Noise of Squeezed-Magnon Mediated Spin Transport, Physical Review Letters 116, 146601 (2016).
- [23] A. Kamra, U. Agrawal, and W. Belzig, Noninteger-spin magnonic excitations in untextured magnets, Physical Review B 96, 020411 (2017).

- [24] K. Agarwal, R. Schmidt, B. Halperin, V. Oganesyan, G. Zaránd, M. D. Lukin, and E. Demler, Magnetic noise spectroscopy as a probe of local electronic correlations in two-dimensional systems, Phys. Rev. B 95, 155107 (2017).
- [25] S. Chatterjee, J. F. Rodriguez-Nieva, and E. Demler, Diagnosing phases of magnetic insulators via noise magnetometry with spin qubits, Physical Review B 99, 104425 (2019).
- [26] B. Flebus and Y. Tserkovnyak, Quantum-Impurity Relaxometry of Magnetization Dynamics, Physical Review Letters 121, 187204 (2018).
- [27] S. P. Wolski, D. Lachance-Quirion, Y. Tabuchi, S. Kono, A. Noguchi, K. Usami, and Y. Nakamura, Dissipationbased quantum sensing of magnons with a superconducting qubit, Phys. Rev. Lett. 125, 117701 (2020).
- [28] F. Casola, T. van der Sar, and A. Yacoby, Probing condensed matter physics with magnetometry based on nitrogen-vacancy centres in diamond, Nature Reviews Materials 3, 1 (2018).
- [29] Z.-X. Liu, H. Xiong, M.-Y. Wu, and Y.-q. Li, Absorption of magnons in dispersively coupled hybrid quantum systems, Physical Review A 103, 063702 (2021).
- [30] Y. Tabuchi, S. Ishino, A. Noguchi, T. Ishikawa, R. Yamazaki, K. Usami, and Y. Nakamura, Coherent coupling between a ferromagnetic magnon and a superconducting qubit, Science 349, 405 (2015).
- [31] G. Burkard, M. J. Gullans, X. Mi, and J. R. Petta, Superconductor–semiconductor hybrid-circuit quantum electrodynamics, Nature Reviews Physics 2, 129 (2020).
- [32] A. Chatterjee, P. Stevenson, S. De Franceschi, A. Morello, N. P. de Leon, and F. Kuemmeth, Semiconductor qubits in practice, Nature Reviews Physics 3, 157 (2021).
- [33] M. M. Nieto, Displaced and squeezed number states, Physics Letters A 229, 135 (1997).
- [34] P. Král, Displaced and squeezed fock states, Journal of Modern Optics 37, 889 (1990).
- [35] L. Trifunovic, F. L. Pedrocchi, and D. Loss, Longdistance entanglement of spin qubits via ferromagnet, Phys. Rev. X 3, 041023 (2013).
- [36] I. C. Skogvoll, J. Lidal, J. Danon, and A. Kamra, Tunable Anisotropic Quantum Rabi Model via a Magnon–Spin-Qubit Ensemble, Physical Review Applied 16, 064008 (2021).
- [37] S. A. Bender and Y. Tserkovnyak, Interfacial spin and heat transfer between metals and magnetic insulators, Physical Review B 91, 140402 (2015).
- [38] S. Takahashi, E. Saitoh, and S. Maekawa, Spin current through a normal-metal/insulating-ferromagnet junction, Journal of Physics: Conference Series 200, 062030 (2010).
- [39] A. Kamra and W. Belzig, Magnon-mediated spin current noise in ferromagnet — nonmagnetic conductor hybrids, Physical Review B 94, 014419 (2016).
- [40] See Supplemental Material for (i) a detailed derivation of the system Hamiltonian and squeezing, (ii) a detailed derivation of the excitation energies, (iii) a detailed derivation of the effective squeezing between the excited state squeezed-magnon vacuum and the ground state squeezed-magnon vacuum, (iv) a description of the details of the numerical simulations as well as the simulation parameters, (v) examination of limits under which the qubit spectroscopy remains linear thereby probing

- the desired equilibrium superposition and how one can resolve the weaker peaks by employing larger Rabi drives, (vi) a discussion about the coherent coupling in the dispersive limit, and (vii) design equations for two different magnon–spin qubit platforms that admit direct dispersive coupling, which includes Refs. [64–78].
- [41] The ground state stability requires $A \geq 2|B| + \chi$ which yields a finite r_a .
- [42] In contrast, the conventional qubit spectroscopy [10, 11] of nonequilibrium superpositions yields peaks separated by the typically smaller quantity χ.
- [43] J. R. Johansson, P. D. Nation, and F. Nori, QuTiP: An open-source Python framework for the dynamics of open quantum systems, Computer Physics Communications 183, 1760 (2012).
- [44] J. R. Johansson, P. D. Nation, and F. Nori, QuTiP 2: A Python framework for the dynamics of open quantum systems, Computer Physics Communications 184, 1234 (2013).
- [45] H.-P. Breuer and F. Petruccione, The Theory of Open Quantum Systems (Oxford University Press, 2007).
- [46] G. Lindblad, On the generators of quantum dynamical semigroups, Communications in Mathematical Physics 48, 119 (1976).
- [47] V. Gorini, A. Kossakowski, and E. C. G. Sudarshan, Completely positive dynamical semigroups of N-level systems, Journal of Mathematical Physics 17, 821 (1976).
- [48] I. I. Rabi, Space Quantization in a Gyrating Magnetic Field, Physical Review 51, 652 (1937).
- [49] Y. Tabuchi, S. Ishino, A. Noguchi, T. Ishikawa, R. Yamazaki, K. Usami, and Y. Nakamura, Quantum magnonics: The magnon meets the superconducting qubit, Comptes Rendus Physique Quantum Microwaves / Micro-ondes Quantiques. 17, 729 (2016).
- [50] D. Zueco, G. M. Reuther, S. Kohler, and P. Hänggi, Qubit-oscillator dynamics in the dispersive regime: Analytical theory beyond the rotating-wave approximation, Physical Review A 80, 033846 (2009).
- [51] This can be done by, for example, employing a larger amplitude of the qubit drive since the qubit excitation increases with the drive [40].
- [52] C. Ciuti and I. Carusotto, On the ultrastrong vacuum Rabi coupling of an intersubband transition in a semiconductor microcavity, Journal of Applied Physics 101, 10.1063/1.2722757 (2007), 081709.
- [53] J. Zou, S. K. Kim, and Y. Tserkovnyak, Tuning entanglement by squeezing magnons in anisotropic magnets, Physical Review B 101, 014416 (2020).
- [54] D. Wuhrer, N. Rohling, and W. Belzig, Theory of quantum entanglement and structure of the two-mode squeezed antiferromagnetic magnon vacuum, Phys. Rev. B 105, 054406 (2022).
- [55] J. Shim, S.-J. Kim, S. K. Kim, and K.-J. Lee, Enhanced magnon-photon coupling at the angular momentum compensation point of ferrimagnets, Phys. Rev. Lett. 125, 027205 (2020).
- [56] A. Kamra, E. Thingstad, G. Rastelli, R. A. Duine, A. Brataas, W. Belzig, and A. Sudbø, Antiferromagnetic magnons as highly squeezed Fock states underlying quantum correlations, Physical Review B 100, 174407 (2019).
- [57] H. Y. Yuan, S. Zheng, Z. Ficek, Q. Y. He, and M.-H. Yung, Enhancement of magnon-magnon entanglement inside a cavity, Phys. Rev. B 101, 014419 (2020).
- [58] V. Azimi Mousolou, Y. Liu, A. Bergman, A. Delin,

- O. Eriksson, M. Pereiro, D. Thonig, and E. Sjöqvist, Magnon-magnon entanglement and its quantification via a microwave cavity, Phys. Rev. B **104**, 224302 (2021).
- [59] S. Sharma, V. A. S. V. Bittencourt, A. D. Karenowska, and S. V. Kusminskiy, Spin cat states in ferromagnetic insulators, Physical Review B 103, L100403 (2021).
- [60] J. Zhao, A. V. Bragas, D. J. Lockwood, and R. Merlin, Magnon squeezing in an antiferromagnet: Reducing the spin noise below the standard quantum limit, Phys. Rev. Lett. 93, 107203 (2004).
- [61] J. Li, S.-Y. Zhu, and G. S. Agarwal, Squeezed states of magnons and phonons in cavity magnomechanics, Phys. Rev. A 99, 021801 (2019).
- [62] M. Elyasi, Y. M. Blanter, and G. E. W. Bauer, Resources of nonlinear cavity magnonics for quantum information, Phys. Rev. B 101, 054402 (2020).
- [63] M. Kounalakis, G. E. W. Bauer, and Y. M. Blanter, Analog quantum control of magnonic cat states on a chip by a superconducting qubit, Phys. Rev. Lett. 129, 037205 (2022).
- [64] T. Holstein and H. Primakoff, Field Dependence of the Intrinsic Domain Magnetization of a Ferromagnet, Physical Review 58, 1098 (1940).
- [65] N. N. Bogoljubov, V. V. Tolmachov, and D. V. Širkov, A New Method in the Theory of Superconductivity, Fortschritte der Physik 6, 605 (1958).
- [66] S. S.-L. Zhang and S. Zhang, Spin convertance at magnetic interfaces, Physical Review B 86, 214424 (2012).
- [67] R. Achilles and A. Bonfiglioli, The early proofs of the theorem of Campbell, Baker, Hausdorff, and Dynkin, Archive for History of Exact Sciences 66, 295 (2012).
- [68] I. I. Rabi, On the Process of Space Quantization, Physical Review 49, 324 (1936).
- [69] Y. Kajiwara, K. Harii, S. Takahashi, J. Ohe, K. Uchida, M. Mizuguchi, H. Umezawa, H. Kawai, K. Ando, K. Takanashi, S. Maekawa, and E. Saitoh, Transmission of electrical signals by spin-wave interconversion in a magnetic insulator, Nature 464, 262 (2010).
- [70] F. D. Czeschka, L. Dreher, M. S. Brandt, M. Weiler, M. Althammer, I.-M. Imort, G. Reiss, A. Thomas, W. Schoch, W. Limmer, H. Huebl, R. Gross, and S. T. B.

- Goennenwein, Scaling Behavior of the Spin Pumping Effect in Ferromagnet-Platinum Bilayers, Physical Review Letters **107**, 046601 (2011).
- [71] M. Weiler, M. Althammer, M. Schreier, J. Lotze, M. Pernpeintner, S. Meyer, H. Huebl, R. Gross, A. Kamra, J. Xiao, Y.-T. Chen, H. Jiao, G. E. W. Bauer, and S. T. B. Goennenwein, Experimental Test of the Spin Mixing Interface Conductivity Concept, Physical Review Letters 111, 176601 (2013).
- [72] L. Schlipf, T. Oeckinghaus, K. Xu, D. B. R. Dasari, A. Zappe, F. F. de Oliveira, B. Kern, M. Azarkh, M. Drescher, M. Ternes, K. Kern, J. Wrachtrup, and A. Finkler, A molecular quantum spin network controlled by a single qubit, Science Advances 3, e1701116 (2017).
- [73] E. Lee-Wong, R. Xue, F. Ye, A. Kreisel, T. van der Sar, A. Yacoby, and C. R. Du, Nanoscale Detection of Magnon Excitations with Variable Wavevectors Through a Quantum Spin Sensor, Nano Letters 20, 3284 (2020).
- [74] J. R. Maze, P. L. Stanwix, J. S. Hodges, S. Hong, J. M. Taylor, P. Cappellaro, L. Jiang, M. V. G. Dutt, E. Togan, A. S. Zibrov, A. Yacoby, R. L. Walsworth, and M. D. Lukin, Nanoscale magnetic sensing with an individual electronic spin in diamond, Nature 455, 644 (2008).
- [75] T. van der Sar, F. Casola, R. Walsworth, and A. Yacoby, Nanometre-scale probing of spin waves using single electron spins, Nature Communications 6, 7886 (2015).
- [76] K. Yang, W. Paul, S.-H. Phark, P. Willke, Y. Bae, T. Choi, T. Esat, A. Ardavan, A. J. Heinrich, and C. P. Lutz, Coherent spin manipulation of individual atoms on a surface, Science 366, 509 (2019).
- [77] L. M. Veldman, L. Farinacci, R. Rejali, R. Broekhoven, J. Gobeil, D. Coffey, M. Ternes, and A. F. Otte, Free coherent evolution of a coupled atomic spin system initialized by electron scattering, Science 372, 964 (2021).
- [78] T. Choi, W. Paul, S. Rolf-Pissarczyk, A. J. Macdonald, F. D. Natterer, K. Yang, P. Willke, C. P. Lutz, and A. J. Heinrich, Atomic-scale sensing of the magnetic dipolar field from single atoms, Nature Nanotechnology 12, 420 (2017).

Supplementary material with the manuscript Resolving nonclassical magnon composition of a magnetic ground state via a qubit by

Anna-Luisa E. Römling, Alejandro Vivas-Viaña, Carlos Sánchez Muñoz, and Akashdeep Kamra

HAMILTONIAN

In this section, we derive the Hamiltonian [Eq. (1)] describing the dispersively coupled magnon and qubit. We start by deriving the ferromagnetic Hamiltonian where we also discuss the squeezing of the isolated magnon. We then focus on the interfacial exchange-mediated interaction between the magnon and the spin qubit.

Magnon

For the ferromagnet, we consider the Zeeman energy induced by an external magnetic field in z-direction, the ferromagnetic exchange interaction between nearest neighbors and a generalized anisotropy term. The total spin Hamiltonian reads [36]

$$\hat{\mathcal{H}}_{F} = |\gamma| \,\mu_{0} H_{0} \sum_{i} \hat{S}_{iz} - J \sum_{\langle i,j \rangle} \hat{\boldsymbol{S}}_{i} \cdot \hat{\boldsymbol{S}}_{j} + \sum_{i} \left[K_{x} \left(\hat{S}_{ix} \right)^{2} + K_{y} \left(\hat{S}_{iy} \right)^{2} + K_{z} \left(\hat{S}_{iz} \right)^{2} \right], \tag{S1}$$

with the gyromagnetic ratio $\gamma < 0$, the applied external field $H_0 e_z$ (with the unit vector in z-direction e_z), the exchange coupling strength J. The spin operator at lattice site i is denoted by \hat{S}_i and $\langle i,j \rangle$ indicates a sum over nearest neighbors. The magnetic anisotropy is parametrized by the factors K_x , K_y and K_z [36, 39]. In the ground state, the spins point in the negative z-direction. We assume only small deviations from that state such that we can operate in the spin wave approximation. This allows us to use the linearized Holstein-Primakoff transformations [64]

$$\hat{S}_{i+} = \sqrt{2S}\hat{a}_i^{\dagger},\tag{S2}$$

$$\hat{S}_{iz} = -S + \hat{a}_i^{\dagger} \hat{a}_i, \tag{S3}$$

with $\hat{S}_{i\pm} = \hat{S}_{ix} \pm i\hat{S}_{iy}$ and the spin magnitude S. The bosonic operator \hat{a}_i^{\dagger} creates a local magnon ("spin flip") at lattice site i. The corresponding Fourier transformation reads

$$\hat{a}_i = \frac{1}{\sqrt{N_F}} \sum_{\mathbf{k}} \hat{a}_{\mathbf{k}} e^{-i\mathbf{k} \cdot \mathbf{r}_i},\tag{S4}$$

where N_F denotes the total number of lattice sites in the ferromagnet. Using the transformations Eq. (S2), Eq. (S3) and Eq. (S4), Skogvoll *et al.* [36] show that, retaining only the uniform $\mathbf{k} = 0$ magnon mode (denoted as $\hat{a}_0 = \hat{a}$), the ferromagnetic Hamiltonian [Eq. (S1)] transforms into

$$\hat{\mathcal{H}}_{F} = A\hat{a}^{\dagger}\hat{a} + B\hat{a}^{2} + B^{*}\hat{a}^{\dagger 2},\tag{S5}$$

with the constants $A = |\gamma| \mu_0 H_0 + (K_x + K_y - 2K_z) S$ and $B = S(K_x - K_y)/2$. This form of the ferromagnetic Hamiltonian [Eq. (S5)] is used in the main text [Eq. (1)].

In the following, we want to discuss the diagonalization of the isolated ferromagnet $\hat{\mathcal{H}}_F$ [Eq. (S5)] which can be achieved with a Bogoliubov transformation [64, 65]

$$\hat{\alpha} = \hat{a}\cosh r + \hat{a}^{\dagger}e^{i\theta}\sinh r. \tag{S6}$$

We denote $\hat{\alpha}$ as the bare squeezed-magnon [22]. Defining the one-mode squeeze operator [4]

$$\hat{S}(\xi) = \exp\left[\frac{\xi^*}{2}\hat{a}^2 - \frac{\xi}{2}\left(\hat{a}^\dagger\right)^2\right],\tag{S7}$$

the relation between the bare squeezed-magnon $\hat{\alpha}$ and the magnon \hat{a} can be expressed as

$$\hat{\alpha}^{\dagger} = \hat{S}(\xi) \,\hat{a}^{\dagger} \hat{S}^{\dagger}(\xi) \,. \tag{S8}$$

The complex squeezing factor $\xi = r \exp(i\theta)$ is dictated by the parameters A and B via

$$tanh (2r) = \frac{2|B|}{A},$$
(S9)

and the phase

$$e^{i\theta} = \frac{B^*}{|B|}. ag{S10}$$

The diagonalized Hamiltonian becomes

$$\hat{\mathcal{H}}_{F} = \omega_{\alpha} \hat{\alpha}^{\dagger} \hat{\alpha} + \frac{\omega_{\alpha} - A}{2},\tag{S11}$$

with the resonance frequency

$$\omega_{\alpha} = \sqrt{A^2 - 4\left|B\right|^2},\tag{S12}$$

which requires $|A| \ge 2|B|$ for stability.

Dispersive Interaction

Here, we consider an interfacial exchange interaction between the spins of the ferromagnet and the spin qubit. A similar contribution to the Hamiltonian is obtained from dipolar interaction between a magnet and an appropriately located spin qubit [24, 35]. The spin Hamiltonian reads [36]

$$\hat{\mathcal{H}}_{\text{int}} = J_{\text{int}} \sum_{l} \hat{\mathbf{S}}_{l} \cdot \hat{\mathbf{s}}_{l}, \tag{S13}$$

where l label the interfacial site, J_{int} is the interfacial coupling strength [37–39, 66], \hat{S} denotes the ferromagnetic spin operator and \hat{s} the spin of the electronic states comprising the qubit. Skogvoll *et al.* [36] show that the spin of the qubit can be written as

$$\hat{\boldsymbol{s}}_l = \frac{|\psi_l|^2}{2} \hat{\boldsymbol{\sigma}},\tag{S14}$$

where ψ_l is the wave function amplitude of the qubit orbital at position l and $\hat{\boldsymbol{\sigma}} = \hat{\sigma}_x \boldsymbol{e}_x + \hat{\sigma}_y \boldsymbol{e}_y + \hat{\sigma}_z \boldsymbol{e}_z$ denotes the Pauli vector with the Pauli matrices $\hat{\sigma}_{x,y,z}$ and unit vectors $\boldsymbol{e}_{x,y,z}$. Following this, they demonstrate that the interaction [Eq. (S13)] can be expressed in the form

$$\hat{\mathcal{H}}_{\text{int}} = J_{\text{int}} \sum_{l} \left[\hat{S}_{lz} \hat{s}_{lz} + \frac{1}{2} \left(\hat{S}_{l+} \hat{s}_{l-} + \hat{S}_{l-} \hat{s}_{l+} \right) \right], \tag{S15}$$

and that the term $\propto \hat{S}_{l+}\hat{s}_{l-} + H.c.$ results in a coherent magnon-qubit exchange coupling. Focusing on the uniform k=0 mode, they obtain the coherent interaction

$$\hat{\mathcal{H}}_{\rm coh} = J_{\rm int} N_{\rm int} |\psi|^2 \sqrt{\frac{S}{2N_F}} \left(\hat{a}^{\dagger} \hat{\sigma}_{-} + \hat{a} \hat{\sigma}_{+} \right), \tag{S16}$$

with the averaged wavefunction $|\psi|^2 = \sum_l |\psi_l|^2 / N_{\text{int}}$. Note that N_{int} denotes the number of interfacial sites. Let's focus on the term $\propto \hat{S}_{lz} \hat{s}_{lz}$ and name that part of the Hamiltonian $\hat{\mathcal{H}}_{\text{int},zz}$ for now. Using Eq. (S3), Eq. (S4) and the z-component of Eq. (S14), we find that $\hat{\mathcal{H}}_{\text{int},zz}$ becomes

$$\hat{\mathcal{H}}_{\text{int},zz} = -\frac{SJ_{\text{int}}N_{\text{int}}|\psi|^2}{2}\hat{\sigma}_z + \frac{J_{\text{int}}}{2N_F} \sum_{l} |\psi_l|^2 \sum_{\boldsymbol{k},\boldsymbol{k}'} \hat{a}_{\boldsymbol{k}}^{\dagger} \hat{a}_{\boldsymbol{k}'} e^{-i(\boldsymbol{k}-\boldsymbol{k}')\cdot\boldsymbol{r}_l} \hat{\sigma}_z. \tag{S17}$$

The first term is a renormalization of the qubit frequency and can be absorbed into the definition of ω_q . We focus on the remaining term naming it $\hat{\mathcal{H}}_{dis}$:

$$\hat{\mathcal{H}}_{\text{dis}} = \frac{J_{\text{int}}}{2N_F} \sum_{l} |\psi_l|^2 \sum_{\mathbf{k}, \mathbf{k}'} \hat{a}_{\mathbf{k}}^{\dagger} \hat{a}_{\mathbf{k}'} e^{-i(\mathbf{k} - \mathbf{k}') \cdot \mathbf{r}_l} \hat{\sigma}_z.$$
 (S18)

A further simplification of this term requires detailed knowledge of the orbital wavefunction ψ_l of the spin qubit. This will depend on the physical system being considered. The final result for this term will also differ when one considers dipolar interaction [24, 35] instead of the exchange coupling considered herein. In order to obtain an estimate and simplify Eq. (S18), we assume $|\psi_l|^2$ to be spatially independent replacing it with its average value $|\psi|^2$. Under this replacement and assuming the ferromagnet to be thin, we may sum over the interfacial sites l obtaining

$$\hat{\mathcal{H}}_{\text{dis}} = \frac{J_{\text{int}} N_{\text{int}}}{2N_F} |\psi|^2 \sum_{\mathbf{k}, \mathbf{k}'} \hat{a}_{\mathbf{k}}^{\dagger} \hat{a}_{\mathbf{k}'} \delta_{\mathbf{k}, \mathbf{k}'} \hat{\sigma}_z = \frac{J_{\text{int}} N_{\text{int}}}{2N_F} |\psi|^2 \sum_{\mathbf{k}} \hat{a}_{\mathbf{k}}^{\dagger} \hat{a}_{\mathbf{k}} \hat{\sigma}_z, \tag{S19}$$

where $\delta_{\mathbf{k},\mathbf{k}'}$ is the Kronecker delta function. Focusing on only the uniform $\mathbf{k} = \mathbf{0}$ mode, we obtain the direct dispersive interaction considered in the main text:

$$\hat{\mathcal{H}}_{\text{dis}} = \frac{J_{\text{int}} N_{\text{int}} |\psi|^2}{2N_F} \hat{a}^{\dagger} \hat{a} \hat{\sigma}_z \equiv \chi \hat{a}^{\dagger} \hat{a} \hat{\sigma}_z, \tag{S20}$$

where we again use the notation \hat{a} for representing the uniform mode.

EXCITATION ENERGIES

As discussed in the main text, the transition of qubit from its ground to excited state can correspond to multiple excitation frequencies ω_{2n} [Eq. (4)] when coupled to an anisotropic ferromagnet. In this section, we present the mathematical details on how to obtain the ground and excited states as well as the transition frequencies between them.

Let's project the full system Hamiltonian $\hat{\mathcal{H}}_{\text{sys}}$ [Eq. (1)] onto the qubit ground state $|g\rangle$ and excited state $|e\rangle$. We denote the reduced Hamiltonians by $\hat{\mathcal{H}}_{m}^{g} = \langle g | \hat{\mathcal{H}}_{\text{sys}} | g \rangle$ and $\hat{\mathcal{H}}_{m}^{e} = \langle e | \hat{\mathcal{H}}_{\text{sys}} | e \rangle$ respectively and obtain

$$\hat{\mathcal{H}}_g = (A - \chi) \,\hat{a}^{\dagger} \hat{a} + B \hat{a}^2 + B^* \hat{a}^{\dagger 2} - \frac{\omega_q}{2},\tag{S21}$$

$$\hat{\mathcal{H}}_e = (A + \chi) \,\hat{a}^{\dagger} \hat{a} + B \hat{a}^2 + B^* \hat{a}^{\dagger 2} + \frac{\bar{\omega_q}}{2}. \tag{S22}$$

We diagonalize Eq. (S21) and Eq. (S22) with the help of Bogoliubov transformations (that have the same form as Eq. (S6)) and obtain

$$\hat{\mathcal{H}}_g = \omega_\alpha^g \hat{\alpha}_g^\dagger \hat{\alpha}_g - \frac{\omega_q}{2} + \frac{\omega_\alpha^g - (A - \chi)}{2},\tag{S23}$$

$$\hat{\mathcal{H}}_e = \omega_\alpha^e \hat{\alpha}_e^\dagger \hat{\alpha}_e + \frac{\omega_q}{2} + \frac{\omega_\alpha^e - (A + \chi)}{2}.$$
 (S24)

We denote the eigenmode of Eq. (S21) as the ground state squeezed magnon $\hat{\alpha}_g$ and the eigenmode of Eq. (S22) as the excited state squeezed-magnon $\hat{\alpha}_e$. They can be obtained by applying the one-mode squeeze operator \hat{S} [Eq. S7]

$$\hat{\alpha}_{g/e}^{(\dagger)} = \hat{S}\left(\xi_{g/e}\right) \hat{a}^{(\dagger)} \hat{S}^{\dagger}\left(\xi_{g/e}\right), \tag{S25}$$

with the complex squeezing factors $\xi_{g/e} = r_{g/e} \exp{(i\theta)}$. The absolute value of the squeezing factors read

$$r_{g/e} = \frac{\operatorname{arctanh}\left(\frac{2|B|}{A \mp \chi}\right)}{2},$$
 (S26)

such that $r_g > r$ and $r_e < r$, considering $\chi > 0$ as assumed in this work. The angle θ is given by $\exp(i\theta) = B^*/|B|$ and is therefore the same in both cases. The eigenenergies ω_{α}^g and ω_{α}^e read

$$\omega_{\alpha}^{g/e} = \sqrt{(A \mp \chi)^2 - 4|B|^2},$$
 (S27)

such that $\omega_{\alpha}^g < \omega_{\alpha}$ and $\omega_{\alpha}^e > \omega_{\alpha}$. Note that the ground state squeezed-magnon requires $A > \chi$ and $A \ge 2|B| + \chi$ for stability.

The ground state is given by the lowest energy state of $\hat{\mathcal{H}}_g$ which is the ground state squeezed-magnon vacuum $|0\rangle_g$. The ground state energy is therefore

$$\omega_0^g = -\frac{\omega_q}{2} + \frac{\omega_\alpha^g - (A - \chi)}{2}.\tag{S28}$$

As discussed in the main text, the qubit can be excited into the excited state squeezed-magnon Fock states $|2n\rangle_e$ (eigenstates of $\hat{\mathcal{H}}_e$). The energy of an excited state $|2n\rangle_e$ reads

$$\omega_{2n}^e = 2n \cdot \omega_\alpha^e + \frac{\omega_q}{2} + \frac{\omega_\alpha^e - (A + \chi)}{2},\tag{S29}$$

where $2n = {}_e\langle 2n|\,\hat{\alpha}_e^\dagger\hat{\alpha}_e\,|2n\rangle_e$. The excitation energy from the ground state $|0\rangle_g$ to an excited state $|2n\rangle_e$ is then given by the energy difference $\omega_{2n}=\omega_{2n}^e-\omega_0^g$ which explicitly reads

$$\omega_{2n} = \omega_q + \frac{\omega_\alpha^e - \omega_\alpha^g}{2} - \chi + 2n \cdot \omega_\alpha^e. \tag{S30}$$

This is Eq. (4) from the main text.

EFFECTIVE SQUEEZING

As discussed in the main text, the qubit coupled to the magnon mode can transition from its ground state $|0\rangle_g$ into different excited states $|2n\rangle_e$ corresponding to the different occupancy n of the magnon mode in the final state. This is because the squeezing of the ground state squeezed-magnon r_g and the excited state squeezed-magnon r_e are different. We state in the main text that the ground state squeezed-magnon vacuum $|0\rangle_g$ and the excited state squeezed-magnon vacuum $|0\rangle_e$ are squeezed with respect to each other by an effective squeezing factor $r_{\rm eff} = r_e - r_g$. This allows us to write the ground state squeezed-magnon vacuum $|0\rangle_g$ as a superposition of excited state squeezed-magnon Fock states $|2n\rangle_e$. In this section, we want to derive the effective squeezing in mathematical detail.

It is necessary to express the ground state $|0\rangle_g$ and the excited states $|2n\rangle_e$ in a common basis. We denote the magnon Fock states by $|n\rangle$. This way, the ground state squeezed-magnon vacuum can be written as

$$|0\rangle_g = \hat{S}\left(\xi_g\right)|0\rangle \tag{S31}$$

and the excited state squeezed-magnon Fock states [18]

$$|2n\rangle_e = \hat{S}(\xi_e)|2n\rangle$$
. (S32)

The squeeze operators $\hat{S}\left(\xi_{g/e}\right)$ have the same form as Eq. (S7) with the squeezing factors $\xi_{g/e}$ [Eq. (S26)]. In order to eliminate the magnon vacuum $|0\rangle$ from Eq. (S31) and establish a connection between the squeezed-magnon vacuum states $|0\rangle_q$ and $|0\rangle_e$, we use the relation

$$|0\rangle = \hat{S}\left(-\xi_e\right)|0\rangle_e. \tag{S33}$$

Note that we exploited the fact that the inverse of the squeezing operator [Eq. (S7)] is $\hat{S}^{-1}(\xi_e) = \hat{S}(-\xi_e)$. Inserting Eq. (S33) into Eq. (S31), we find a relationship between the squeezed-magnon vacuum states $|0\rangle_q$ and $|0\rangle_e$ via

$$|0\rangle_{q} = \hat{S}\left(\xi_{q}\right)\hat{S}\left(-\xi_{e}\right)|0\rangle_{e}. \tag{S34}$$

Since the operator $\hat{S}(\xi_g)\hat{S}(-\xi_e)$ is a product of two matrix exponentials [see Eq. (S7)], we proceed by evaluating the corresponding Baker-Campbell-Hausdorff formula [67]

$$e^{\hat{X}}e^{\hat{Y}} = e^{\hat{Z}},\tag{S35}$$

with the operators

$$\hat{X} = \frac{\xi_g^*}{2} \hat{a}^2 - \frac{\xi_g}{2} \left(\hat{a}^\dagger \right)^2, \tag{S36}$$

$$\hat{Y} = \frac{\xi_e}{2} \left(\hat{a}^{\dagger} \right)^2 - \frac{\xi_e^*}{2} \hat{a}^2, \tag{S37}$$

and $\hat{Z} = \hat{X} + \hat{Y} + \frac{1}{2} \left[\hat{X}, \hat{Y} \right] + \dots$ In order to determine the exponential \hat{Z} , we need to evaluate the commutator $\left[\hat{X}, \hat{Y} \right]$ and obtain

$$\left[\hat{X}, \hat{Y}\right] = \frac{\xi_g^* \xi_e - \xi_g \xi_e^*}{4} \left[\hat{a}^2, \left(\hat{a}^\dagger\right)^2\right]. \tag{S38}$$

The factor in front of the bosonic commutator can be written in polar representation as

$$\xi_g^* \xi_e - \xi_g \xi_e^* = r_g r_e \left(e^{-i(\theta_g - \theta_e)} - e^{i(\theta_g - \theta_e)} \right), \tag{S39}$$

which becomes zero if $\theta_g = \theta_e$. This is true in our case, since the angle θ is only defined by B which is the same for both squeezed-magnons, hence $\theta_g = \theta_e$. Therefore, the exponential \hat{Z} is simply $\hat{Z} = \hat{X} + \hat{Y}$ and the product of squeeze operators becomes

$$\hat{S}(\xi_g)\,\hat{S}(-\xi_e) = \exp\left[\frac{(\xi_g - \xi_e)^*}{2}\hat{a}^2 - \frac{\xi_g - \xi_e}{2}(\hat{a}^\dagger)^2\right],\tag{S40}$$

which is equal to the squeeze operator $\hat{S}(\xi_g - \xi_e)$. Let us denote this as an effective squeezing $\xi_{\text{eff}} = (r_g - r_e) \exp{(i\theta)}$ and express the ground state squeezed-magnon vacuum as

$$|0\rangle_{q} = \hat{S}\left(\xi_{\text{eff}}\right)|0\rangle_{e}. \tag{S41}$$

This is the relation we use to obtain Eq. (3) from the main text.

QUBIT SPECTROSCOPY SIMULATION

In this section, the technicalities of the qubit spectroscopy are described in more detail. For the spectroscopy, we aim to simulate the dynamics of the dispersively coupled qubit and magnon. For this, we consider Lindblad Master equations [45, 46] and implement a coherent microwave drive for the qubit, such that the full Hamiltonian used for the simulation is time dependent and reads

$$\hat{\mathcal{H}}_{\text{sim}} = A\hat{a}^{\dagger}\hat{a} + B\hat{a}^{2} + B^{*}\hat{a}^{\dagger 2} + \frac{\omega_{q}}{2}\hat{\sigma}_{z} + \chi\hat{a}^{\dagger}\hat{a}\hat{\sigma}_{z} + \Omega_{d}\cos(\omega_{d}t)(\hat{\sigma}_{+} + \hat{\sigma}_{-}). \tag{S42}$$

The qubit is considered to be an open quantum system with the Lindblad dissipator $\hat{C} = \sqrt{\gamma_q} \hat{\sigma}_z$ and decay rate γ_q . In order to perform the numerics, the Python package QuTip [43, 44] is used. For the measurement simulations, we initialize the system in the ground state of the system Hamiltonian $\hat{\mathcal{H}}_{\rm sys}$ [Eq. (1)] and drive the qubit with the frequency ω_d . Then, we let the system evolve until the time $T = 15/\gamma_q$ and measure the qubit response $\langle \hat{\sigma}_+ \hat{\sigma}_- \rangle$. Note that the time evolution is calculated with numerical integration and the time T is chosen large enough such that the system reaches a steady state. To account for possible oscillations, the qubit excitation $\langle \hat{\sigma}_+ \hat{\sigma}_- \rangle$ is averaged in the time interval $t \in [t_0, T]$ with $t_0 = 14/\gamma_q$. In that interval, we take $N_{\rm step}$ integration steps such that the discrete time steps fulfill $t_{n+1} = t_n + \Delta t$ with $\Delta t = (N_{\rm step} \gamma_q)^{-1}$. The numerical value of the steady state qubit excitation can now be expressed as

$$\langle \hat{\sigma}_{+} \hat{\sigma}_{-} \rangle_{\text{st}} = \frac{1}{N_{\text{step}}} \sum_{t_{n}}^{T} \langle \hat{\sigma}_{+} \hat{\sigma}_{-} \rangle (t_{n}).$$
 (S43)

The qubit drive ω_d is swept over a frequency range (in the main text, we choose the range such that the frequencies ω_0 to ω_2 [Eq. (4)] are covered). For each drive frequency ω_d , we plot the steady state qubit excitation $\langle \hat{\sigma}_+ \hat{\sigma}_- \rangle_{\rm st}$ resulting in the desired qubit spectroscopy with excitation peaks. This allows us to probe the qubit excitation frequencies.

Whenever we perform a simulation with the direct dispersive coupling χ , we fix the simulation parameters of the bare squeezed-magnon frequency $\omega_{\alpha}/2\pi = 5\,\mathrm{GHz}$, the qubit frequency $\omega_q/2\pi = 10\,\mathrm{GHz}$, the qubit dissipation $\gamma_q/2\pi = 1\,\mathrm{GHz}$ and the Rabi frequency $\Omega_d/2\pi = 0.14\,\mathrm{GHz}$. This way, we have a detuning between the bare squeezed-magnon and qubit of $\Delta = 5\,\mathrm{GHz}$. We choose the simulation parameters in a way that does not disturb the magnon state and allows for a perturbative treatment. For instance, the Rabi frequency Ω_d is small enough such that we operate in the linear regime and do not drive the magnon through the qubit. Furthermore, we choose the combination of parameters ($\omega_{\alpha}, \gamma_q, \Omega_d$), such that peaks are well separated and resolvable. The simulation in Fig. 4 are generated with a direct disperive coupling strength of $\chi = 2\,\mathrm{GHz}$.

RESOLVING EXCITATION PEAKS

In this section, we want to discuss some limitations of the qubit spectroscopy measurement protocol. We first explore a wider range of Rabi frequency Ω_d . This way, we test if the system is driven out of equilibrium and therefore determine the maximum values of Ω_d that allow to probe the magnetic ground state. We then proceed to discuss the experimental subtleties when resolving further peaks around resonance frequencies ω_4 , ω_6 [Eq. (6)] and so on. Since the corresponding transitions into the states $|2n\rangle_e$ are suppressed by a factor of $p_{2n} = |c_{2n}|^2$ [Eq. (5)] we outline experimental strategies that may enable resolving these weak and well-separated peaks.

Linear response and weak Rabi drive

As explained in section above, we choose the Rabi frequency Ω_d small enough such that the measurement process is only a perturbation on the system state. By driving the qubit at sufficiently large Rabi frequencies Ω_d , the magnon is driven through the qubit reaching a non-equilibrium state.

An approximate analytical expression for each of the resonance peaks can be achieved by viewing each transition $|0\rangle_g \to |2n\rangle_e$ as a two level system, labeled by lowering operator $\hat{\sigma}_{2n}$, and calculating the steady-state qubit population. The master equation [45] that we employ for this purpose is

$$\partial_t \hat{\rho}_{2n} = -i \left[\left(\omega_{2n} - \omega_d \right) \hat{\sigma}_{2n}^{\dagger} \hat{\sigma}_{2n} + \frac{\Omega_d}{2} \left(c_{2n}^* \hat{\sigma}_{2n} + c_{2n} \hat{\sigma}_{2n}^{\dagger} \right), \hat{\rho}_{2n} \right] + \gamma_q \mathcal{D} \left[\hat{\sigma}_{2n} \right] \left(\hat{\rho}_{2n} \right), \tag{S44}$$

where $\hat{\rho}_{2n}$ is the corresponding density matrix and $\mathcal{D}\left[\hat{\sigma}_{2n}\right]\left(\hat{\rho}_{2n}\right)$ denotes the dissipator $\mathcal{D}\left[\hat{\sigma}_{2n}\right]\left(\hat{\rho}_{2n}\right) = \hat{\sigma}_{2n}\hat{\rho}_{2n}\hat{\sigma}_{2n}^{\dagger} - \frac{1}{2}\left\{\hat{\sigma}_{2n}^{\dagger}\hat{\sigma}_{2n},\hat{\rho}_{2n}\right\}$. The factors c_{2n} [Eq. (5)] take into account that the transition $|0\rangle_g \rightarrow |2n\rangle_e$ is suppressed by $p_{2n} = |c_{2n}|^2$. The steady state solution of the qubit population is then given by [4]

$$\langle \hat{\sigma}_{2n}^{\dagger} \hat{\sigma}_{2n} \rangle_{\text{st}} = p_{2n} \frac{(\Omega_d/2)^2}{(\gamma_q/2)^2 + (\omega_{2n} - \omega_d)^2 + 2p_{2n} (\Omega_d/2)^2}.$$
 (S45)

When $\Omega_d^2 \ll \gamma_q^2/2p_{2n}$ is fulfilled, the qubit response scales with Ω_d^2 . This is what we denote as the linear response regime.

In Fig. S1, we show the contrast resulting from simulations for a wide range of Rabi frequencies $\Omega_d \in \gamma_q \cdot [10^{-2}, 10^0]$ for three different values of direct dispersive coupling strength $\chi/\omega_q = 0.15$, $\chi/\omega_q = 0.2$ and $\chi/\omega_q = 0.25$. For comparison, we also plot the theory value expected from Eq. (7). For small Ω_d the contrast from simulations is constant with increasing Ω_d and corresponds to the theory value. For large $\Omega_d > \gamma_q/10$ corresponding to the considered value of r, the contrast increases and is therefore not representative of the magnetic ground state composition marking the limit of the linear response regime quantified by Eq. (S45) above.

In Fig. S2 we plot the average ground state squeezed-magnon number $\langle \hat{\alpha}_g^{\dagger} \hat{\alpha}_g \rangle_{\rm st}$ as well as the steady-state qubit population $\langle \sigma_+ \sigma_- \rangle_{\rm st}$ at resonance frequencies ω_0 and ω_2 . The average ground state squeezed-magnon number $\langle \hat{\alpha}_g^{\dagger} \hat{\alpha}_g \rangle_{\rm st}$ is almost zero at small Ω_d , in consistence with the magnon system being in its ground state. Due to the definition of $\hat{\alpha}_g$ and the excitation into the $|0\rangle_e$ and $|2\rangle_e$, the expectation values $_e \langle 0| \hat{\alpha}_g^{\dagger} \hat{\alpha}_g |0\rangle_e = \sinh^2(r_{\rm eff})$ and $_e \langle 2| \hat{\alpha}_g^{\dagger} \hat{\alpha}_g |2\rangle_e = 2\cosh^2(r_{\rm eff}) + 3\sinh^2(r_{\rm eff})$ are non-zero giving rise to the non-equilibrium steady-state when the Rabi drive becomes large. Consistent with our conclusion above, maintaining a weak Rabi drive in the linear regime [Eq. (S45)] ensures that the magnon system maintains its ground state.

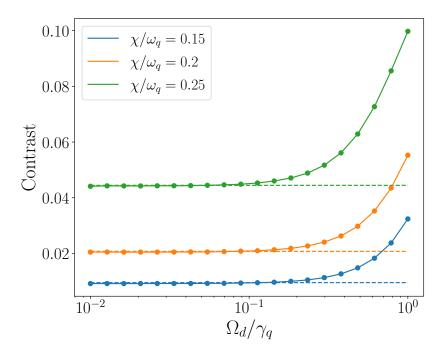


FIG. S1. The contrast between the peaks at ω_2 and ω_0 is plotted against the Rabi frequency Ω_d for three different values of the direct dispersive coupling strength $\chi/\omega_q=0.15$, $\chi/\omega_q=0.2$ and $\chi/\omega_q=0.25$. The bold lines represent the contrast generated from simulations and the dashed lines the corresponding theory value for the contrast. The remaining parameters are fixed by $\omega_\alpha/\omega_q=0.5$, r=0.2 and $\gamma_q/\omega_q=0.1$.

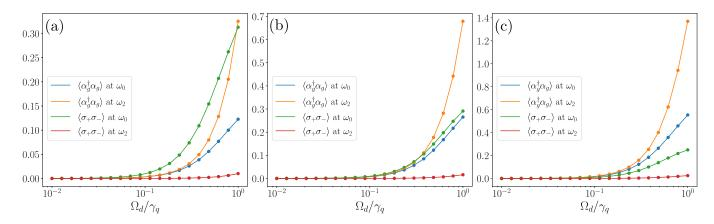


FIG. S2. The steady state ground state squeezed-magnon number evaluated at the system resonance frequencies ω_0 and ω_2 as well as the qubit population, also evaluated at ω_0 and ω_2 , are plotted against the Rabi frequency for three values of direct dispersive coupling strength (a) $\chi/\omega_q = 0.15$, (b) $\chi/\omega_q = 0.2$ and (c) $\chi/\omega_q = 0.25$. The remaining parameters are fixed by $\omega_\alpha/\omega_q = 0.5$, r = 0.2 and $\gamma_q/\omega_q = 0.1$.

Resolving Further Peaks ω_{2n}

In the main text, we address how to resolve the first non-trivial peak at resonance frequency ω_2 . In the following, we want to address the experimental subtleties when resolving the further peaks at frequency ω_{2n} associated with the transition $|0\rangle_g \to |2n\rangle_e$ for n > 1. Since the excitation probability p_{2n} is suppressed with larger n, the amplitudes of the corresponding excitation peaks in the qubit spectroscopy decrease by the evaluated contrast [Eq. (5)] from one peak to the next. The main point is that since these peaks are well-separated in frequency, we can use larger Rabi drives for probing subsequent peaks without violating the excitation linearity discussed above. We demonstrate this point by simulating the qubit spectroscopy of ω_4 peak explicitly.

In Fig. S3 we show the steady state qubit excitation $\langle \sigma_+ \sigma_- \rangle_{\rm st}$ at resonance frequencies ω_0 , ω_2 and ω_4 . In the

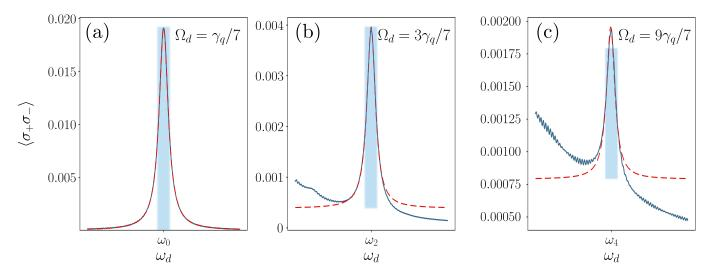


FIG. S3. Steady state qubit population vs. drive frequency. The spectra around the peaks at ω_0 , ω_2 and ω_4 are simulated with different values of the Rabi frequency: $\Omega_d = \gamma_q/7$ for ω_0 , $\Omega_d = 3\gamma_q/7$ for ω_2 and $\Omega_d = 9\gamma_q/7$ for ω_4 . The bold lines are the simulation data, the dashed lines the Lorentzian fits and the bars represent the theory values. The theory bars have been multiplied by Ω_d^2 for ω_2 and ω_4 to account for the larger Rabi drives employed.

simulations, we probe each of the excitation peaks employing different Rabi frequencies Ω_d : $\Omega_d = \gamma_q/7$ for ω_0 , $\Omega_d = 3\gamma_q/7$ for ω_2 and $\Omega_d = 9\gamma_q/7$ for ω_4 . Since the qubit excitation scales as $\sim \Omega_d^2$ in the linear response regime [Eq. (S45)], we can define the experimental contrast for the first non-trivial peak

$$c_{\text{experiment}} = \frac{\langle \hat{\sigma}_{+} \hat{\sigma}_{-} \rangle_{\text{st}} \left(\omega_{d} = \omega_{2} \right) / \Omega_{d,2}^{2}}{\langle \hat{\sigma}_{+} \hat{\sigma}_{-} \rangle_{\text{st}} \left(\omega_{d} = \omega_{0} \right) / \Omega_{d,0}^{2}}, \tag{S46}$$

where $\Omega_{d,2n}$ denotes the Rabi frequency used to resolve the peak at ω_{2n} for n=0,1. An analogous expression can be defined for the contrast of the second non-trivial peak. The simulation reported in Fig. S3 shows that employing a larger Rabi drive for the non-overlapping peaks allows to correctly obtain the contrast due to the equilibrium superposition from even the weak peaks. As a last note, the resolution of the peaks becomes better with smaller qubit dissipation γ_q since the overlap between excitation peaks decreases.

COHERENT COUPLING IN THE DETUNED LIMIT

Spin qubits couple dispersively and coherently with the magnet (see section). Superconducting qubits on the other hand couple coherently to the magnonic mode and have no "in-built" direct dispersive coupling to magnets [30, 49]. However, one obtains an effective dispersive interaction arising from the coherent coupling in the highly detuned limit [10, 11]. This is why we want to discuss the coherent coupling in the dispersive limit and address the question if the magnon composition of an equilibrium squeezed magnetic ground state can be resolved with this kind of interaction as well. We also want to discuss if the measurement mechanism obtained from direct dispersive coupling is perturbed when coherent coupling is present. This effective dispersive interaction has been detailed in the text book [3] or, for instance, in [11] and [10].

Let's consider a ferromagnet with anisotropies as discussed section . We now assume that the local magnon \hat{a} ("spin flip") and a qubit $\hat{\sigma}$ are coupled coherently via Rabi interaction [48, 68] and that there is no direct dispersive coupling. The corresponding system Hamiltonian has the form

$$\hat{\mathcal{H}}_{\text{sys, SC}} = A\hat{a}^{\dagger}\hat{a} + B\hat{a}^2 + B^*\hat{a}^{\dagger 2} + \frac{\omega_q}{2}\hat{\sigma}_z + g\left(\hat{a}^{\dagger} + \hat{a}\right)\left(\hat{\sigma}_+ + \hat{\sigma}_-\right). \tag{S47}$$

where the coherent coupling strength is denoted by g. We transform into the eigenbasis of the ferromagnet by using the Bogoliubov transformation [Eq. (S6)] such that the system Hamiltonian becomes

$$\hat{\mathcal{H}}_{SC,\alpha} = \omega_{\alpha} \hat{\alpha}^{\dagger} \hat{\alpha} + \frac{\omega_{q}}{2} \hat{\sigma}_{z} + \tilde{g} \hat{\alpha}^{\dagger} \hat{\sigma}_{-} + \tilde{g}^{*} \hat{\alpha} \hat{\sigma}_{+} + \tilde{g} \hat{\alpha}^{\dagger} \hat{\sigma}_{+} + \tilde{g}^{*} \hat{\alpha} \hat{\sigma}_{-}, \tag{S48}$$

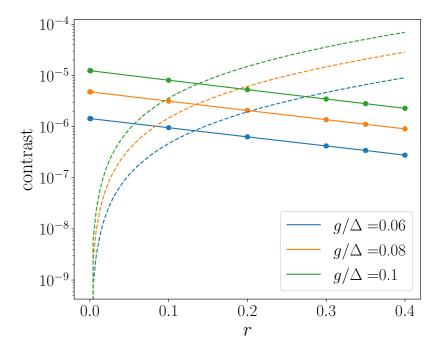


FIG. S4. The contrast between the first non-trivial peak and the trivial peak is plotted as a function of the squeezing r for several values of coherent coupling g. We compare simulation data (points and solid lines) with the expected contrast arising from the analytic model with direct dispersive coupling $\chi = \tilde{\chi}$ [Eq. (S49)]. The fixed parameters are $\omega_{\alpha}/2\pi = 5 \, \mathrm{GHz}$, $\omega_q/2\pi = 10 \, \mathrm{GHz}$, $\gamma_q/2\pi = 10 \, \mathrm{MHz}$ and $\Omega_d/2\pi = 1.4 \, \mathrm{MHz}$.

where the modified coupling strength reads $\tilde{g} = g\left(\cosh r - e^{i\theta}\sinh r\right)$ and we neglected the vacuum energy. The dispersive limit is defined by a large detuning of the boson and the qubit while being relatively weakly coupled such that $\tilde{g} \ll |\omega_q - \omega_\alpha|$. This way the modes do not hybridize and the interaction can be treated perturbatively. Now if we do not neglect the fast rotating terms (taking into account the full Hamiltonian $\hat{\mathcal{H}}_{SC,\alpha}$ [Eq. (S48)]) performing perturbation theory will lead to a diagonal term $\propto \hat{\alpha}^{\dagger}\hat{\alpha}$ and non-diagonal terms $\propto \hat{\alpha}^2$, $(\hat{\alpha}^{\dagger})^2$. Assuming \tilde{g} to be real, Zueco *et al.* [50] have shown that the dispersive limit beyond the rotating wave approximation leads to an effective frequency shift in the qubit frequency

$$\tilde{\chi} = \tilde{g}^2 \left(\frac{1}{\omega_q - \omega_\alpha} + \frac{1}{\omega_q + \omega_\alpha} \right). \tag{S49}$$

The Hamiltonian $\mathcal{H}_{\text{sys,SC}}$ [Eq. (S47)] cannot be easily treated analytically. For this reason, we perform the numerical simulations of the qubit spectroscopy as described in the main text and the SM. We keep the bare squeezed-magnon frequency $\omega_{\alpha}/2\pi = 5\,\mathrm{GHz}$ and the qubit frequency $\omega_{q}/2\pi = 10\,\mathrm{GHz}$. For higher precision, we choose a small qubit decay rate $\gamma_q/2\pi=10\,\mathrm{MHz}$ and Rabi frequency $\Omega_d/2\pi=1.4\,\mathrm{MHz}$. We find that there is a non-trivial peak arising around $\omega_d \approx \omega_q + 2\omega_\alpha$ which we analyse varying the squeezing r and the coherent coupling g. In Fig. S4, we show the contrast plotted against the squeezing r for several values of g. We compare the contrast resulting from the numerical simulations (points and solid lines) with the contrast arising from the analytic theory with direct dispersive coupling (dashed lines) given by Eq. (5) from the main text. We find that the numerical calculation with coherent coupling and the analytic model arising from direct dispersive coupling $\chi = \tilde{\chi}$ [Eq. (S49)] do not match. While the contrast in our analytic model is equal to zero in the absence of squeezing and increasing with larger squeezing r, the contrast in the numerical data is nonzero for r=0 and decreasing with larger r. We therefore conclude that the peak is unrelated to the measurement mechanism obtained with direct dispersive coupling and stems from another higher order process arising from the counter rotating terms. This shows that the direct dispersive coupling χ is essential for resolving the nonclassical magnon number composition of the magnetic ground state. The previous method [10] for resolving nonequilibrium superpositions using an effective dispersive coupling $\tilde{\chi}$ does not work for equilibrium nonclassical superpositions [18].

Lastly, we want to explore what happens when a qubit is coupled via direct dispersive interaction and coherent interaction. Thereby, we address the question if the coherent coupling perturbs the measurement mechanism obtained

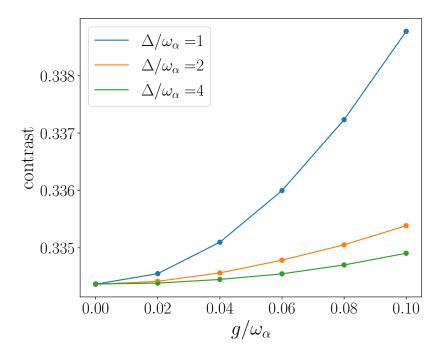


FIG. S5. The contrast between the first non-trivial peak and the trivial peak is plotted as a function of coherent coupling g for several values of magnon-qubit detuning $\Delta = \omega_q - \omega_\alpha$. The data are obtained by simulating the qubit spectra under the evolution of $\hat{\mathcal{H}}_{\text{full}}$ [Eq. (S50)] and determining the height of the two peaks via Lorentzian fits. We fix the simulation parameters by $\omega_\alpha/2\pi = 5 \,\text{GHz}$, r = 0.45, $\chi/2\pi = 2 \,\text{GHz}$, $\gamma_q/2\pi = 1 \,\text{GHz}$ and $\Omega_d/2\pi = 0.14 \,\text{GHz}$.

from direct dispersive coupling when the bare squeezed-magnon frequency ω_{α} and the bare qubit frequency ω_{q} are far detuned. For this reason, we consider the full Hamiltonian

$$\hat{\mathcal{H}}_{\text{full}} = A\hat{a}^{\dagger}\hat{a} + B\hat{a}^{2} + B^{*}\hat{a}^{\dagger 2} + \frac{\omega_{q}}{2}\hat{\sigma}_{z} + \chi\hat{a}^{\dagger}\hat{a}\hat{\sigma}_{z} + g\left(\hat{a}^{\dagger} + \hat{a}\right)\left(\hat{\sigma}_{+} + \hat{\sigma}_{-}\right),\tag{S50}$$

which contains the ferromagnet with anisotropies, the qubit, and both direct and coherent coupling between the magnon \hat{a} and the qubit. Since the Hamiltonian $\hat{\mathcal{H}}_{\text{full}}$ is not analytically tractable, we analyse it numerically using our established qubit spectroscopy simulations as discussed in section . In Fig. S5, we show the contrast between the first non-trivial peak and the trivial peak arising from the numerical simulations as a function of g at different values of the magnon-qubit detuning $\Delta = \omega_q - \omega_\alpha$. We vary the detuning by changing the bare qubit frequency ω_q . The rest of the parameters are fixed by $\omega_\alpha/2\pi = 5\,\text{GHz}$, r = 0.45, $\chi/2\pi = 2\,\text{GHz}$, $\gamma_q/2\pi = 1\,\text{GHz}$ and $\Omega_d/2\pi = 0.14\,\text{GHz}$. For a detuning of $\Delta = 5\,\text{GHz}$ the deviation in the contrast caused by the coherent coupling is less than $1.5\,\%$ for $g = 0.5\,\text{GHz}$ which is already at the limit between weak coupling and strong coupling regime. For a larger detuning of $\Delta = 10\,\text{GHz}$ and $\Delta = 20\,\text{GHz}$ the curves are more flat in the range of g that we consider. We therefore conclude that the perturbation caused by the coherent coupling is insignificant for weak coupling strengths g and that the influence of the coherent coupling can be suppressed using larger detuning Δ .

EXPERIMENTAL PLATFORMS FOR DIRECT DISPERSIVE COUPLING

In this section, we examine some available experimental setups that may achieve the direct dispersive coupling between a qubit and magnetic insulator. In section above, we have derived the direct dispersive interaction $\hat{\mathcal{H}}_{\text{dis}} = \chi \hat{a}^{\dagger} \hat{a} \hat{\sigma}_z$ [Eq. (S20)] starting with an exchange coupling Hamiltonian. The direct dispersive term arises from the z-components of the spin-spin interaction $\propto \hat{S}_z \hat{\sigma}_z$ and its strength is given by

$$\chi = \frac{J_{\rm int} N_{\rm int}}{2N_{\rm F}} \left| \psi \right|^2, \tag{S51}$$

with the interfacial exchange coupling strength $J_{\rm int}$, the number of interfacial lattice sites $N_{\rm int}$, the number of lattice sites in the ferromagnet $N_{\rm F}$ and the averaged spin qubit wave function $|\psi|^2$.

Here, we consider two types of qubits that provide the interaction $\propto \hat{S}_z \hat{\sigma}_z$ noting that better candidates might have escaped our attention or become available in the near future. First, we focus on semiconducting quantum dots that interact through exchange coupling with magnets [32]. We then turn our attention to nitrogen-vacancy (NV) defects in diamond which may interact with magnets via magnetic dipole-dipole coupling [28]. From experimentally known parameters and set-ups, we provide design equations for optimizing these platforms and achieving a desired χ .

Exchange interaction

Semiconducting quantum dots implement spin exchange interaction, see Ref. [32] for a review. Such a magnet–spin qubit system focusing on coherent interaction has been detailed in Ref. [36]. Considering this set-up, we evaluate the direct dispersive interaction between far detuned spin qubit and magnon. Assuming the qubit wave function to be localized in N_{layer} monolayers of an equally thin ferromagnet with N_{int} interfacial sites, such that $|\psi|^2 = 1/N_{\text{F}}$ with $N_{\text{F}} = N_{\text{layers}}N_{\text{int}}$, the direct dispersive coupling strength becomes

$$\chi = \frac{J_{\text{int}}}{2N_{\text{lavers}}^2 N_{\text{int}}},\tag{S52}$$

which is increasing with decreasing size of the magnet. From spin-pumping experiments [69–71], we take the interfacial exchange coupling $J_{\rm int} \approx 10\,{\rm meV}$ for our estimation. Assuming $N_{\rm layer} = 5$ monolayers and $N_{\rm int} = 1000$ interfacial sites yields $\chi = 0.00002 \cdot J_{\rm int} = 0.3\,{\rm GHz}$. Reducing the number of interfacial sites to $N_{\rm int} = 100$ results in an increased direct dispersive coupling strength $\chi = 3\,{\rm GHz}$. In conclusion, Eq. (S52) above provides the necessary design equation that could be employed in engineering a desired value of the direct dispersive coupling. It also shows that smaller system sizes on the nanoscale are needed for this.

Dipole-dipole coupling

NV center defects in diamond interact with other spins through dipole-dipole interaction [28]. In the supplemental information of Ref. [72], the interaction between NV center and network spins is modeled by a term $\propto \hat{S}_z \hat{\sigma}_z$. This motivates us to examine the suitability of NV centers as spin qubits for our measurement protocol.

A general expression of magnetic dipole-dipole interaction between an NV center and a magnetic insulator reads

$$\hat{\mathcal{H}}_{dd} = \frac{\mu_0}{4\pi} \sum_{l} \frac{1}{r_l^3} \left[\mathbf{M}_l \cdot \mathbf{m}_{NV} - 3 \left(\mathbf{M}_l \cdot \hat{\mathbf{r}}_l \right) \left(\mathbf{m}_{NV} \cdot \hat{\mathbf{r}}_l \right) \right], \tag{S53}$$

where $m_{\rm NV}$ is the magnetic moment of the NV center, M_l denotes the magnetic moment of interfacial lattice site l and r_l is the distance between the NV center and interfacial lattice site l. \hat{r}_l is a unit vector in the direction of the line joining $m_{\rm NV}$ and M_l . We want to bring Eq. (S53) into the form of Eq. (S13) in order to estimate an effective $J_{\rm int}$ from dipole-dipole interaction which we denote by $J_{\rm dd}$. This is accomplished by positioning the NV center such that its spin and displacement from the magnet are orthogonal to each other. Assuming the magnetic moments $m_{\rm NV}$ and M_l to be in plane and the unit vectors \hat{r}_l to be out of plane, Eq. (S53) becomes

$$\hat{\mathcal{H}}_{dd} = \frac{\mu_0}{4\pi} \sum_{l} \frac{\gamma_l \gamma_{NV}}{r_l^3} \hat{\mathbf{S}}_l \cdot \hat{\mathbf{s}}_{NV}, \tag{S54}$$

where $\hat{\mathbf{S}}_l$ and $\hat{\mathbf{s}}_{\text{NV}}$ denote the spin operators at lattice site l and the NV center, and γ_l and γ_{NV} are the corresponding gyromagnetic ratios. Finally, assuming that the distances r_l are approximately equal $r_l \approx r$ and that the gyromagnetic ratios of the interfacial sites are the same $\gamma_l = \gamma$, we obtain the effective coupling

$$J_{\rm dd} = \frac{\mu_0}{4\pi} \frac{\gamma \gamma_{\rm NV}}{r^3},\tag{S55}$$

which strongly depends on the distance r. The distance between the probe and the NV center in experiments can be around $r=100\,\mathrm{nm}$ [73] down to tens of nanomometers [74, 75]. For electron spins $\gamma_l=\gamma_\mathrm{NV}=\gamma_e$, we estimate an effective interfacial coupling strength of $J_\mathrm{dd}\approx0.16\,\mathrm{peV}$ for a distance of $r=100\,\mathrm{nm}$ and $J_\mathrm{dd}\approx0.16\,\mathrm{neV}$ for $r=10\,\mathrm{nm}$. Even the larger value $J_\mathrm{dd}\approx0.16\,\mathrm{neV}$ is 10 orders smaller than the interfacial coupling J_int from exchange interaction. This would result in a direct dispersive coupling strength in the order of $\chi \propto 0.1\,\mathrm{Hz}$. We conclude that this coupling strength is too weak and magnetic dipole-dipole interaction is not suitable for our purposes.

However, newly developed protocols and qubits employing electron spin resonance (ESR) and single spins offer the potential for smaller distances. In such studies, the magnetic dipolar interactions have been found to play an important role and may admit significant direct dispersive interactions [76–78].